Design and experimental study of an indirect heat pump distillation system for treating high-concentration saline wastewater

Jingxiang Lin, Guoliang Qin*, Cheng Jia

*School of Energy and Power Engineering, Xi'an Jiaotong University, Xi'an 710049, China, Tel. +86 15991652855;
emails: glqin@xjtu.edu.cn (G. Qin), linjingxiang0825@stu.xjtu.edu.cn (J. Lin), gyjiacheng@stu.xjtu.edu.cn (C. Jia)*

ABSTRACT

Conventional distillation systems such as multi-effect evaporation and multi-stage flash evaporation are subject to problems of high energy consumption and additional corollary equipment, and energy-efficient mechanical vapor re-compression (MVR) systems have problems of compressor size and cost. An indirect heat pump distillation system for treating high-concentration saline wastewater is developed that consists of a refrigerant heat pump system and a double-effect forced circulation system. Using refrigerant as the heat pump working fluid can significantly reduce the volume flow rate of the compressor design under the same compressor outlet energy head. Through a comparative analysis based on the first law of thermodynamics, it was found that using the R-22 refrigerant and the countercurrent feeding method can achieve better results than those achieved by R-134a and the downstream feeding method. A temperature of 25°C is the optimum feeding temperature, and it allows the system to have a better compressor performance and a smaller heat transfer area. A comparison of the experimental and exergy analysis results shows that the energy efficiency of the designed system is close to that of the MVR system in the literature, and the designed system has advantages in both compressor selection and system operation.

Keywords: Distillation system; Heat pump; Experimental study; Exergy analysis

1. Introduction

Copious amounts of wastewater with high concentrations of inorganic salts are discharged by chemical engineering industries. Inorganic salts contained in some wastewater possess recycling value. Direct discharge of this wastewater leads to water pollution and a waste of resources. According to the literature [1,2], biological, ion exchange, membrane and evaporation methods are commonly used for the treatment of high-concentration salt-containing wastewater.

Among the thermal methods, multi-effect evaporation (MEE) and multi-stage flash (MSF) evaporation are commonly used. The MSF method has high energy consumption and equipment investments, and the MEE has problems such as high energy consumption, additional corollary equipment, and high operating costs. Aussenac et al. [3] developed a distillation system named mechanical vapor re-compression (MVR). The MVR system can recycle the energy of secondary vapor, thus achieving a higher thermal efficiency compared with MEE and MSF [4]. A detailed mathematical model and performance analysis of a single-stage and double-stage MVR system are given by Ahmadi et al. [5]. Double-stage MVR can achieve a 3.3% energy savings compared with the single-stage MVR system. In the field of crystallization, double-stage MVR can achieve zero emissions [6]. The MVR system only requires a steam heat source at the system startup, so during the system operation, electricity seems to be the only source of energy. The MVR system can be

* Corresponding author.

combined with renewable energy. Helal and Al-Malek [7] studied an MVR system combined with solar energy with a fresh water capacity of 120 m³ d⁻¹. Zejli et al. [8] presented a wind/PV-driven MVR system, and the produced domestic water cost was approximately 0.7 € m⁻³.

The water vapor compressor is the core device of the MVR system. Currently, water vapor compressors are mainly centrifugal, screw and root compressors. Centrifugal compressors are often used in cases with a large amount of evaporation; due to the characteristics of the turbomachinery and water vapor properties, centrifugal compressors have a small single-stage compression ratio, high discharge temperature and droplet sensitivity. Dust or droplets in the working fluid easily cause impeller failure [9] and are prone to surge when the inlet flow rate is reduced. Screw and root compressors are volume compressors that allow two-phase compression, and screw compressors are the most commonly used among these types. Compared with centrifugal compressors, screw compressors have the advantage of a large pressure ratio, but the flow rate of the steam working fluid is relatively low. Roots compressors have a simple structure, and they generally only operate under high-temperature conditions with a low flow rate and low-temperature rise to the boiling point; in addition, the pressure ratio is not high, and the efficiency is low. At present, the use of water vapor as a working medium still requires more development. Lachner et al. [10] reported that water vapor as a refrigerant in the vapor compression process is less economical than Freon refrigerant R-134a. Compared with the MVR system, refrigerant compressors are much smaller than steam compressors with the same heating power because refrigerants have a higher density than steam, and the energy-carrying capacity per unit volume of refrigerant is approximately 100 times more than that of water vapor.

This paper presents a new evaporation saltwater distillation device that has a similar energy recovery effect to that of MVR. In contrast to the MVR method, the presented method uses a compression refrigerant heat pump as the heat source. In addition, MVR systems employ the direct heat pump method, in which secondary steam is recovered as a heat source directly. The technique of using a refrigerant heat pump to recover secondary steam is called an indirect heat pump method. Few research studies have been reported in this field to our knowledge. Rice and Chau [11] proposed a desalination system using a hydraulic refrigerant compressor in 1997 and improved the efficiency of freeze desalination over its previous value. Slesarenko [12] studied a desalination system using an absorption heat pump that could reduce the water production cost by 2%–2.5%. Slesarenko [13] designed a vapor compression heat pump desalination system and used thermodynamic analysis to show its good energy efficiency. Chen and Huang [14] discussed the feasibility of this method and showed that R-12 was not suitable as the heat pump refrigerant. Attia [15] proposed and provided a detailed description and thermal analysis of a desalination system with a vapor compression heat pump using R-22 as the working medium. Recently, Attia [16] designed a heat pump seawater desalination system using a passive vacuum generation system and compared the advantages and disadvantages of different refrigerants. From this brief literature review, it can be seen that

there are advantages of using refrigerant as the heat pump working medium.

Thermodynamic analysis methods can be used to analyze the thermodynamic properties of the system quantitatively. Exergy analysis, which is the application of the second law of thermodynamics, can be used to evaluate the system's available energy utilization, especially in the case of a seawater desalination system [17]. Spiegler and El-Sayed [18] optimally designed a brackish water treatment system using exergy analysis, which proved the powerful efficacy of this approach. In a membrane distillation system, exergy analysis has achieved good results in the analysis of system energy consumption and economic evaluation [19]. Kahraman and Cengel [20] thermodynamically analyzed a large MSF distillation plant in a gulf area. They found that the highest exergy destruction (77.7%) occurs within the MSF unit and that the system's exergy efficiency is very low: only 4.2%. Piacentino and Cardona [21,22] applied thermoeconomic analysis to the MEE process and discussed solutions for optimization and energy saving. Jin et al. [23] studied a seawater desalination process unit that operates on the vapor compression flash method and used exergy analysis to identify modifications that would improve the performance of the system. These literature studies illustrate that the exergy analysis method plays an important role in the field of thermal seawater desalination. However, to our knowledge, the literature contains no reports on the exergy analysis of a vapor compression heat pump distillation system. This article details our design of an indirect heat pump distillation system for treating high-concentration saline wastewater and the analysis of the system according to the first and second laws of thermodynamics.

In this paper, the process design and performance of the heat pump distillation system with refrigerant vapor compression are studied. This paper is the first to apply an indirect heat pump evaporation system to deal with concentrated brine, and the use of an experimental study and exergy analysis methods to study the performance and loss distribution of the system represents a novel contribution of this paper. The system described has the following advantages:

- It is capable of recovering the heat from secondary steam and has lower energy consumption than MEE and MSF systems.
- In contrast to MVR systems, this system uses a refrigerant heat pump cycle to recover the latent heat of the secondary steam. Because the refrigerant has a higher energy carrying capacity per unit volume than steam, we can design a smaller compressor under the same power capability. By choosing a compressor with a high-pressure ratio when dealing with materials with high boiling point elevation, this method can significantly reduce compressor manufacturing and maintenance costs.
- Electricity is the only energy source of this system, which is suitable for areas where steam heat sources are expensive and electricity is cheaper. Since the heat pump cycle is a closed-loop, the system is also safer and friendly to operate.

A detailed mathematical model is developed based on the mass and energy conservation equations to study the

system performance under different working conditions. The power consumption, performance and total heat exchanger area of the heaters are the parameters for judging the merits of the system. Moreover, ammonium sulfate wastewater is the concentrated brine for system treatment. Comparing the advantages and disadvantages of different refrigerants, feeding methods and design conditions, the best design parameters for the system are determined. Then, we build an experimental device to verify the calculation results and compare the results with the MVR system.

2. System description and mathematical model

2.1. System description

The specific refrigerant indirect heat pump distillation system with the countercurrent feeding method is shown in Fig. 1, where the dashed line represents the gas and the solid line represents the liquid. The ammonium sulfate wastewater from feed tank 15 enters the second effect forced circulation at ambient temperature and is then sent into heater 2 by the circulation pump. Here, the water vapor is condensed

Table 1
Experimental device and measuring equipment parameters

| Name of the device	Main parameters	Manufacturer
Compressor	VR125KS-TFP-52E	Emerson Copeland (Suzhou, China)
Heater 1	Shell and tube heat exchanger $A1 = 6$ m^2	Customized
Heater 2	Shell and tube heat exchanger $A2 = 5$ m^2	Customized
Heater 3	Shell and tube heat exchanger $A3 = 8$ m^2	Customized
Heater 4	Shell and tube heat exchanger $A4 = 1$ m^2	Customized
Flash evaporator 1	$\Phi = 0.8$ m, H (height) = 1.5 m	Customized
Flash evaporator 2	$\Phi = 1.2$ m, H (height) = 1.5 m	Customized
Circulation pump 1	$q = 15$ m^3 h^{-1}, H (head) = 10 m	Kangerda (Wenzhou, China)
Circulation pump 2	$q = 15$ m^3 h^{-1}, H (head) = 10 m	Kangerda (Wenzhou, China)
Absolute pressure sensor of heat pump circulation	Range: 0–3.0 MPa; currency: 0.5%	MEACON (Hangzhou, China)
Relative pressure sensor of heat pump circulation	Range: –0.100–0.100 MPa; currency: 0.25%	Tiankang (Shanghai, China)
Temperature sensor	Range: –50.0°C–150.0°C; currency: ±(0.30 + 0.005|T|)°C	MEACON (Hangzhou, China)
Waste water flow meter	Range: 0.01–20 m^3 h^{-1}; currency: 1.0%	Certeon
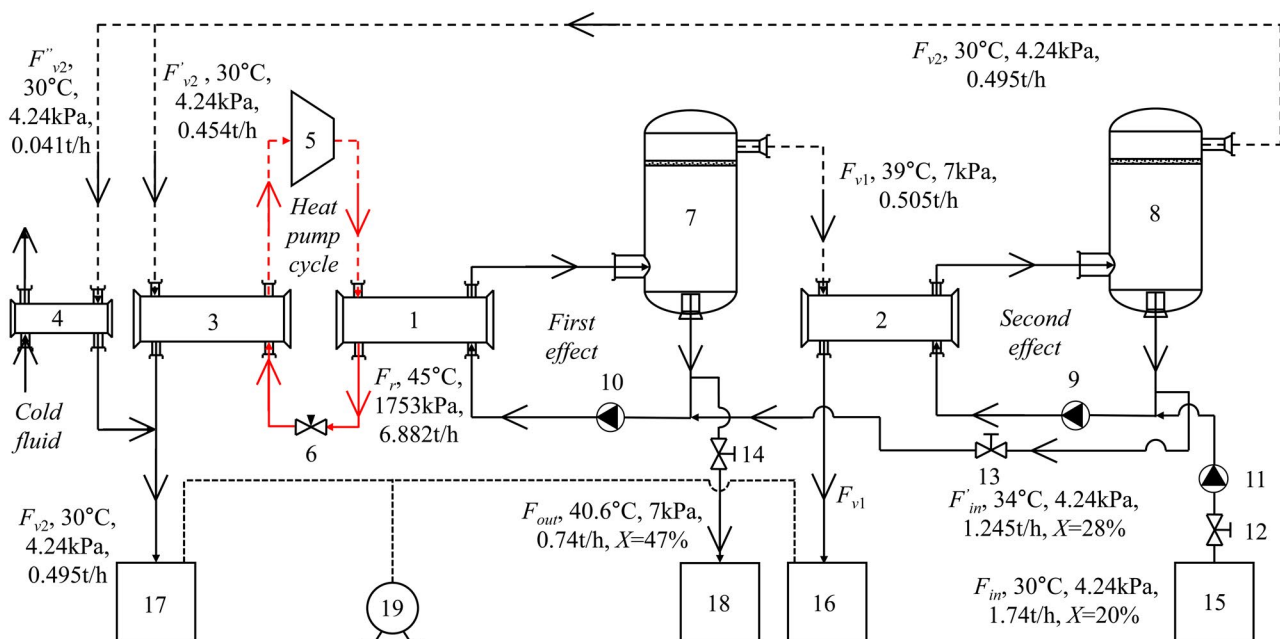
Fig. 1. Refrigerant vapor compression heat pump distillation system with a design evaporation rate of 1 t h^{-1} (countercurrent feeding method). 1, 2, 3, 4-shell-and-tube heat exchangers (heaters); 5-compressor; 6-throttle valve; 7, 8-flash evaporator; 9, 10-forced circulation pump; 11-feed pump; 12, 13, 14-flow control valve; 15-feed tank; 16, 17-pure water tank; 18-centrifuge; 19-vacuum pump.

to liquid and enters pure water tank 16. Absorbing the latent heat of the secondary vapor from the first effect, the hot wastewater enters flash evaporator 8. The flashers are under vacuum due to the action of vacuum pump 19, which allows the solution to evaporate at lower temperatures. Because of the abrupt decrease in pressure, water vapor is formed. The flashed-off vapors are sent separately to heat pump evaporator 3 and compensation condenser 4, and the condensed saturated liquid water is mixed and enters pure water tank 17. The function of compensation condenser 4 is to absorb the latent heat of the secondary vapor out of the second effect that cannot be condensed by the heat pump evaporator. Most of the concentrated brine out of flash evaporator 8 is recirculated to heater 2, and a small amount of concentrated brine is discharged into the first effect, mixed with the recirculation-concentrated brine and then pumped to heater 1 (heat pump condenser). Here, the refrigerant out of compressor 5 releases latent heat to heat the brine. Then, the heated brine solution is sent to flasher 7 for evaporation, and the brine reaches the outlet concentration that can be crystallized. Subsequently, a small part of the slurry out of the first effect forced circulation is discharged into centrifuge 18 to separate the crystals from the brine, and the remaining concentrate continues to circulate and evaporate. When the feed is downstream, the feed solution enters from the first effect forced circulation, and the concentrated liquid is discharged from the second effect. The rest of the process is the same as the countercurrent feed process.

Mass and energy conservation equations are established to help analyze the performance of the system. Then, we establish the experimental device to verify the accuracy of the calculation results.

2.2. Mathematical model of the system

This paper makes the following assumptions before deriving the calculation model:

- System works under steady-state conditions.
- Energy losses in flash evaporators and heat exchangers are not considered.
- Specific enthalpy at the inlet and outlet of the expansion valve is unchanged.
- Concentrated brine leaving the shell sides of both heaters is in the saturated liquid phase.

2.2.1. Mass balance for the system

Take the countercurrent feed process as an example. The total mass conservation equation of the system is given by:

$$F_{in} = F_{v2} + F'_{in} \tag{1}$$

$$F'_{in} = F_{v1} + F_{out} \tag{2}$$

$$F_{v2} = F'_{v2} + F''_{v2} \tag{3}$$

The conservation equation of the solute for a solution is:

$$F_{in} \cdot X_{in} = F'_{in} \cdot X'_{in} = F_{out} \cdot X_{out} + M \tag{4}$$

where F is the mass flow rate, kg s^{-1}; X is the salt mass concentration, %; M is the crystalline salt, kg s^{-1}; the subscripts in, out, $v1$ and $v2$ represent the inlet, outlet, vapor of the first effect and vapor of the second effect, respectively. F'_{in} denotes the concentrated brine after the first evaporation, F'_{v2} and F''_{v2} denote secondary vapor from the second effect entering heat exchangers 3 and 4, respectively.

2.2.2. Energy balance for the heat pump system

The *p-h* diagram of the heat pump cycle is shown in Fig. 2, where positions 1′, 2″, 3′ and 4 represent the refrigerant state at the compressor inlet, compressor outlet, heat pump condenser (heater 3) outlet and inlet of the heat pump condenser evaporator (heater 1), respectively. The energy balance equations for heater 1 and heater 3 are as follows:

$$Q_1 = F_{h1} \cdot \left(Cp_{h1} \cdot T_{h1,out} - Cp_{h1} \cdot T_{h1,in} \right) = F_r \cdot \left(h''_2 - h'_3 \right) \tag{5}$$

$$Q_3 = F'_{v2} \cdot \gamma_{v2} = F_r \cdot \left(h'_1 - h_4 \right) \tag{6}$$

where Q is the heat power of the heat exchanger, kW, and Cp is the constant-pressure specific heat capacity, kJ kg^{-1} K^{-1}. T is the temperature and needs to be converted to units of K in the calculation, and γ is the latent heat of vaporization at temperature T_v, kJ kg^{-1}. T_v is the saturation temperature under the corresponding pressure, and thus γ_{v2} represents the latent heat of vaporization of water vapor under T_{v2}. h is the specific enthalpy, kJ kg^{-1}; the subscripts b and r represent the brine and refrigerant; and $h_{j,in}$ and $h_{j,out}$ refer to the inlet and outlet of heater j, respectively. The Cp of the ammonium sulfate wastewater can be calculated by [24]:

$$Cp = Cp_w \cdot (1 - X) + Cp_s \cdot X \tag{7}$$

where Cp_w is the specific heat capacity of water, which is equal to 4.18 kJ kg^{-1} K^{-1}, and Cp_s is the specific heat capacity of ammonium sulfate, which is approximately 1.7 kJ kg^{-1} K^{-1}. The relationship between T_b and the *j*th effect T_v is given by the following:
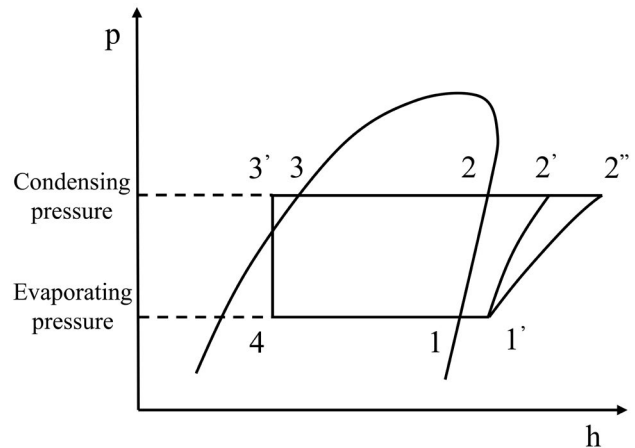

Fig. 2. *p-h* diagram of the heat pump cycle.

$$T_{bj} = T_{vj} + BPE_j \tag{8}$$

where BPE is the boiling point elevation of the solution and can be calculated as follows [24]:

$$BPE_j = f_j \left(0.0027 X_j^2 - 0.0053 X_j + 0.6194 \right) \tag{9}$$

where X_j is the solute's percent mass concentration of the jth effect. The correction factor f_j is defined as:

$$f_j = 0.0162 \frac{T_{vj}^2}{\gamma_{vj}} \tag{10}$$

The adiabatic compression process of the compressor is $1'–2'$ in Fig. 2, where $1'–2''$ is the actual process. The relationship between the total compressor power W_{com} (unit: kW) and the adiabatic compressor power W_{ad} is:

$$\frac{W_{ad}}{W_{com}} = \eta_{com} \tag{11}$$

$$W_{com} = F_r \cdot \left(h_2'' - h_1' \right) = Q_1 - Q_3 \tag{12}$$

$$W_{ad} = \frac{\kappa}{\kappa - 1} R_r T_1' \left[\left(\frac{p_2}{p_1} \right)^{\frac{\kappa-1}{\kappa}} - 1 \right] = F_r \cdot \left(h_2' - h_1' \right) \tag{13}$$

where η_{com} is the isentropic efficiency of the compressor, κ is the heat capacity ratio of the compressor's working fluid, R_r is the gas constant of the compressor's working fluid, and p_2 and p_1 are the outlet pressure and inlet pressure of the compressor.

For the indirect heat pump distillation system, increasing the saturated condensing temperature of the heat pump working fluid can increase the heat released while also increasing the compressor pressure ratio (ratio of outlet pressure to inlet pressure), which will affect the operation of the compressor. In order to describe the coupling relationship between the heat released by the heat pump and the pressure ratio of the compressor, we introduce the parameter α (unit: K kJ^{-1} kg^{-1}) to represent the performance index of the compressor [25] to evaluate the performance of the compressor in the system, which can be described as follows:

$$\alpha = \frac{\Delta T \cdot \gamma_{rc}}{p_{out} / p_{in}} = \frac{\left(T_c - T_e \right) \cdot \gamma_{rc}}{\varepsilon} \tag{14}$$

where ε is the compressor pressure ratio; the subscripts c and e represent condensation and evaporation, respectively, and γ_{rc} represents the latent heat of the refrigerant under the condensing pressure. The dimensions of this parameter can be obtained as follows [25]:

$$\alpha^* = \left(\frac{\left(T_c - T_e \right) \cdot \gamma_{rc}}{T^* \cdot R_g T^*} \right) \bigg/ \varepsilon \tag{15}$$

where R_g (unit: kJ kg^{-1} K^{-1}) is the gas constant of the refrigerant and $T^* = (0.81–0.83) \cdot T_{cr}$ [25], where T^* is the characteristic temperature and T_{cr} is the critical temperature. In the heat pump cycle, a higher value of α^* indicates better performance of the compressor.

2.2.3. Energy balance for the forced circulation system

As is shown in Fig. 1, the feed F_{in} is first sent into the second effect and mixed with the circulating fluid. The mass conservation equations of the jth effect are:

$$F_{hj} - F_{vj} = F_{ej,out} \tag{16}$$

$$F_{in} + F_{e2,out} - F_{in}' = F_{h2} \tag{17}$$

$$F_{in}' + F_{e1,out} - F_{out} = F_{h1} \tag{18}$$

where the subscript ej,out indicates the outlet of the flash evaporator of the jth effect.

The energy balance equation for heater 2 can be described as follows:

$$Q_2 = F_{h2} \cdot \left(Cp_{h2} \cdot T_{h2,out} - Cp_{h2} \cdot T_{h2,in} \right) = F_{v1} \cdot \gamma_{v1} \tag{19}$$

And the energy balance equation for the flash evaporator of the jth effect is:

$$F_{vj} \cdot \gamma_{vj} = F_{hj} \cdot Cp_{hj,out} \cdot T_{hj,out} - F_{ej} \cdot Cp_{ej,out} \cdot T_{ej,out} \tag{20}$$

The power of the circulation pump can be calculated by [24]:

$$W_{pump,j} = F_{hj} \cdot \frac{\Delta P_{hj}}{\left(\rho_{hj} \cdot \eta_{pump} \cdot 1,000 \right)} \tag{21}$$

where ρ_{hj} (unit: kg m^{-3}) is the density of the circulating liquid and ΔP_{hj} (unit: kPa) is the pressure loss to be overcome by the circulation pump, which is given as follows:

$$\Delta P_{hj} = 2 K_{PT} \cdot L \cdot v_T^{1.8} + 2.5 \rho \cdot v_T^2 \tag{22}$$

where K_{PT} can be calculated by:

$$K_{PT} = 0.092 \rho^{0.8} \cdot \mu^{0.2} \cdot d_i^{-1.2} \tag{23}$$

2.2.4. Heat transfer model

The heat transfer equation of the heaters is given by the following:

$$Q_j = A_j \cdot U_j \cdot \Delta T_{LMTD,hj} \tag{24}$$

where A is the heat transfer area, m^2; $\Delta T_{LMTD,hj}$ represents the logarithmic mean temperature difference of the jth heat exchanger; and U is the overall coefficient of heat transfer in units of kW m^{-2} °C^{-1} and can be calculated as follows:

$$U = \frac{1}{1/k_o + R_o + R_i \cdot d_o / d_i + d_o / (d_i \cdot k_i) + d_o / (2\lambda_{wall}) \cdot \ln(d_o / d_i)}$$ (25)

where k is the convective heat transfer coefficient, kW m^{-2} °C^{-1}; R is the fouling resistance; d is the diameter, m; λ_{wall} is the thermal conductivity of the tube, kW m^{-1} °C^{-1}; and the subscripts o and i define the outside and inside of the tubes, respectively.

2.2.5. Exergy analysis

The exergy of the ammonium sulfate solution fluid is the composition of the physical and chemical exergy. Physical exergy is the maximum useful work that can be converted when the system and the environment reach a binding equilibrium. It is caused by the thermal imbalance between the system and the environment. Chemical exergy refers to the maximum useful work that can be converted when the system and the environment change from a binding equilibrium state to a nonbinding equilibrium state. It is caused by the imbalance of chemical composition between the system and the selected environment. Chemical exergy is divided into diffusion exergy due to concentration differences and exergy generated by a chemical reaction between substances. The system studied in this paper does not have a chemical reaction; thus, chemical exergy refers specifically to diffusion exergy. The fluid exergy is calculated as follows [26,27]:

$$e = e_{ph} + e_{ch} = \int_{T_0,P}^{T,P} Cp \cdot \left(1 - \frac{T}{T_0}\right) dT + \int_{T_0,P_0}^{T_0,P} v dP + \bar{R}T_0 \sum_1^k x_{i0} \ln \frac{\alpha_{i0}}{\alpha_i^0}$$ (26)

where e_{ph} and e_{ch} are specific physical and chemical exergy expressed separately, kJ kg^{-1}; v is the specific volume, m^3 kg^{-1}; T_0 and P_0 are the pressure and temperature at the binding equilibrium state; x_{i0} is the molar fraction of component i; and α_i^0 is the activity of component i at the binding equilibrium state. Parameter α_i^0 is the activity of component i at the nonbinding equilibrium state. The ammonium sulfate solution is composed of the solute ammonium sulfate and solvent water, and thus the summation limit "k" is 2.

The refrigerant and water vapor in the system are pure substances, regardless of the influence of changes in the chemical exergy. Because the enthalpy and entropy parameters of water vapor and gaseous refrigerant are easy to find, the equation of the ideal gas is used to calculate its exergy:

$$e = (h - h_0) - T_0 \cdot (s - s_0)$$ (27)

In this paper, the ammonium sulfate solution is regarded as an incompressible fluid. Thus, Eq. (25) can be simplified to:

$$e = Cp\left[T - T_0 - T_0 \ln\left(\frac{T}{T_0}\right)\right] + v(P - P_0) + \bar{R}T_0 \sum_1^k x_{i0} \ln \frac{\alpha_{i0}}{\alpha_i^0}$$ (28)

The final discharged wastewater is the crystal slurry solution. Its exergy is calculated as the sum of the solution exergy and the crystal exergy. The calculation method of crystal exergy is:

$$e_s = v T_0 R_s \ln \frac{\alpha_s'}{\alpha_s^0}$$ (29)

where v is the total number of ions, α_s' is the activity of saturated wastewater.

Exergy destruction and exergy efficiency are commonly used as criteria for evaluating the thermodynamic performance of systems. The exergy destruction diagram of the device i is shown in Fig. 3. The calculation equations for exergy destruction and exergy efficiency are:

$$E_{di} = \sum_1^n E_{in} - \sum_1^n E_{out}$$ (30)

$$\eta_E = \frac{\sum_1^n E_{out}}{\sum_1^n E_{in}}$$ (31)

where E_d represents exergy destruction and η_E means exergy efficiency.

3. Calculation results and analysis

To determine the proper feeding method and heat pump working fluid, we use the MATLAB program to design and calculate the operating parameters of the system. Some parameters need to be given before the calculation, such as system total evaporation flow rate F_v, feeding temperature and concentration T_{in} and X_{in}, discharge concentration X_{out}, the second effect saturated evaporation temperature of water vapor T_{v2} and adiabatic efficiency of the compressor η. To reduce the power consumption of the compressor, the minimum heat transfer temperature difference of each heat exchanger is assumed to be 5°C. The subcooling and superheating of the heat pump cycle are both 2°C. Among these parameters, we assume that the base parameters $F_v = 1$ t h^{-1}, $\eta = 75\%$, $T_{in} = 20$°C, $T_{v2} = 30$°C, $X_{in} = 20\%$, $X_{out} = 47\%$. The concentration of the discharged saturated ammonium sulfate solution is approximately 45%, and the remaining solutes become crystals and are discharged along with the
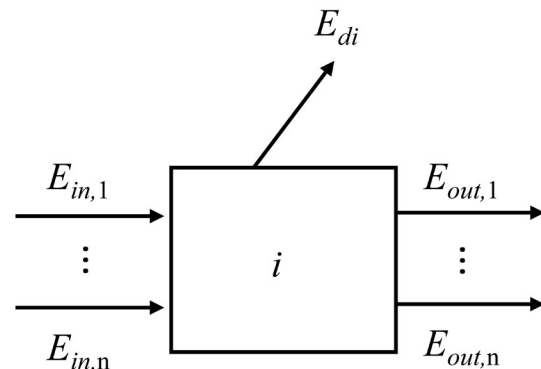

Fig. 3. Exergy balance diagram of device i.

solution. T_{in} and T_{v2} are used as variables to study the system performance.

Because the intermediate effect discharge concentration cannot be determined, we use iterative calculations to calculate its value. The specific calculation method is shown in Fig. 4.

This paper compares the effects of the most commonly used refrigerants R22 and R134a on the market and different feeding modes on the system operating parameters. Fig. 5 shows that the power W_{com} and performance index α^* of the compressor vary with feeding temperature. The finding indicates that a higher feeding temperature could result in lower compressor power consumption. From Eq. (13) we know that the reduction in compressor power consumption is caused by a decrease in the compressor pressure ratio. The temperature difference between the saturated condensing temperature and the saturated evaporating temperature of the heat pump cycle is also reduced, which makes the effect on the compressor performance index small.
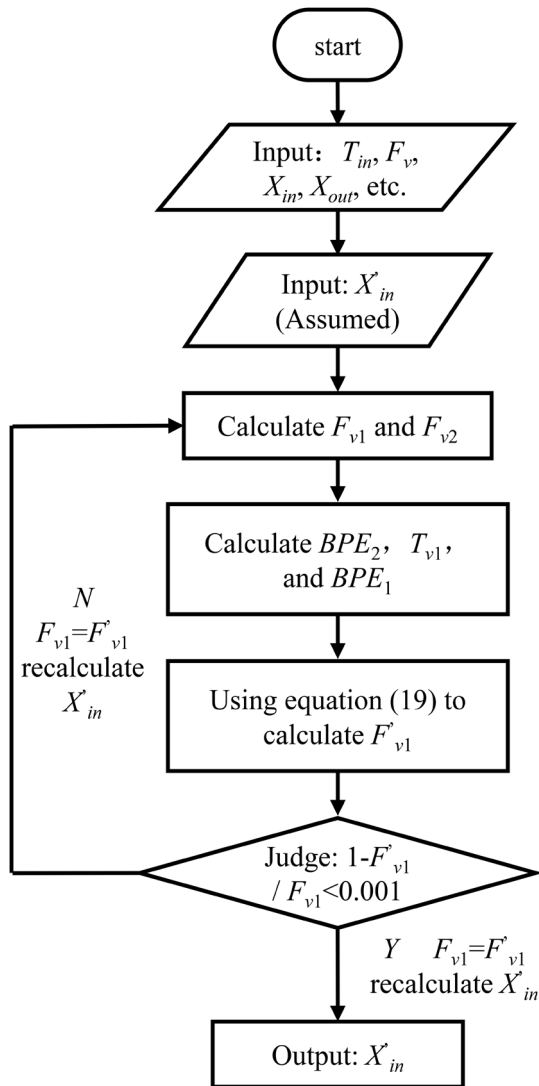
We can determine from Fig. 6 that the total heat transfer area continues to increase with increasing feeding temperature because the heat pump saturated condensing temperature decreases and saturated evaporation temperature increases. An increase in the feeding temperature will raise the temperature of the solution at the inlet of heater 2, and the temperature difference of heater 1, heater 2 and heater 3 will become smaller. However, the assumed system evaporation rate is constant, which means that the heat released by the heat pump does not change. As a result, the total heat exchange area of the heaters will increase with increasing feeding temperature, and the rate of increase is greater beyond 25°C. Taking the R-22 refrigerant and countercurrent feeding method as an example, the compressor power consumption only decreased by 2.5%. Considering an ambient temperature of approximately 25°C, the heat exchange area and the power consumption of the compressor
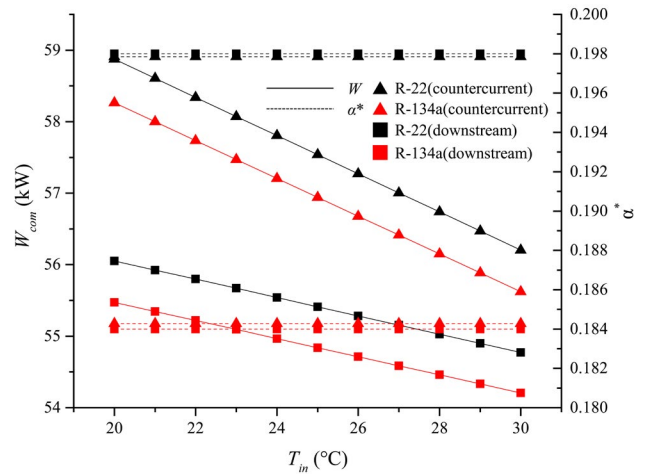

Fig. 5. Compressor power and performance index as a function of feeding temperature with different refrigerants and feeding methods.

Fig. 4. Calculation method for the intermediate effect discharge concentration X'_{in}.
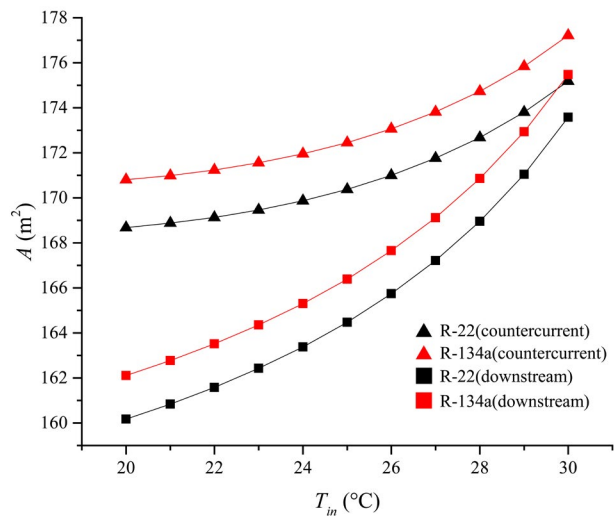

Fig. 6. Total heat transfer area as a function of feed temperature with different refrigerants and feeding methods.

are more reasonable, and thus 25°C will be selected as the feed temperature for the experimental design.

As evident in Fig. 7, with an increasing second effect, saturated evaporation temperature, the power consumption of the compressor increases, but the performance index gradually decreases. When the second effect saturated evaporation temperature increases, the saturation temperature corresponding to the inlet and outlet pressures of the compressor increases simultaneously. At the same time, we know from Fig. 2 that the specific enthalpy of the 1′–2″ process increases, which explains why the power consumption of the compressor increases. However, the compressor's pressure ratio change is more severe than the temperature difference, so the performance index decreases. As shown in Fig. 8, increasing the second effect saturated evaporation temperature causes a reduction in the total heat transfer area.
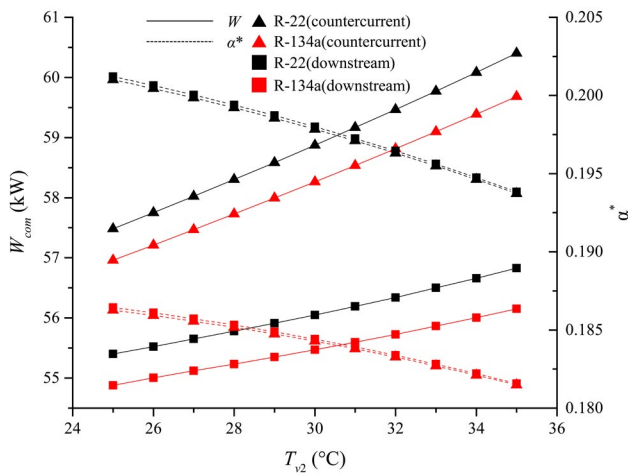

Fig. 7. Compressor power and performance index as a function of the second effect saturated evaporation temperature of water vapor with different refrigerants and feeding methods.
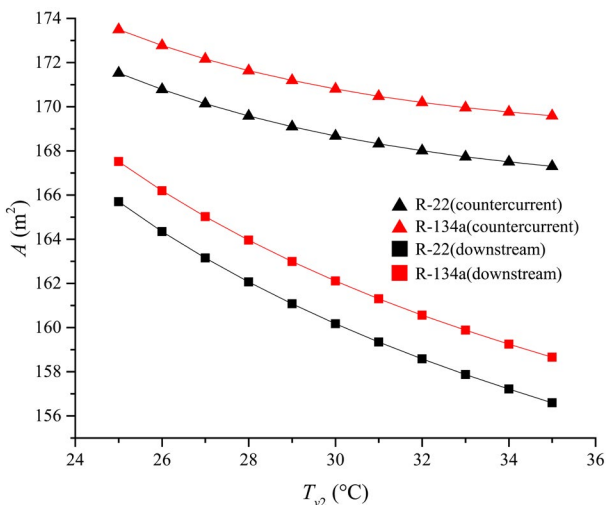

Fig. 8. Total heat transfer area as a function of the second effect saturated evaporation temperature with different refrigerants and feeding methods.

Consequently, if the second effect, saturated evaporation temperature is low, then the vacuum should be relatively high. The system needs better sealing, and the heat exchanger area is large, so a large upfront investment is required. In contrast, a higher second effect saturated evaporation temperature leads to more power consumption and increases the energy investment.

According to the comparative analysis above, using refrigerant R-134a achieves a lower compressor power consumption, but the performance index of the compressor is much lower than that of R-22. In addition, the use of R-22 as the working fluid may result in a smaller heat transfer area, which is also proved in Section 2.3 of a previous study [28]. The difference in the feeding method has little effect on the performance index of the compressor; however, the power of the compressor and total heat transfer area are significantly lower when the countercurrent feed method is used. In general, using R-22 as the working medium and using the countercurrent feed method can achieve better-operating parameters for this system.

4. Experimental study and exergy analysis

Through the previous calculation analysis, a heat pump distillation system with a countercurrent vapor compression and R-22 as the working medium was established. The experimental device designed in this paper has an evaporation capacity of approximately 100 kg h⁻¹. A commercially available Copeland scroll compressor is chosen as the heat pump compressor of this system. Heaters 1, 2, 3, and 4 use horizontal shell-and-tube heat exchangers, and the tubes are flooded by the ammonium sulfate solution. The specific experimental equipment parameters are shown in Table 1.

The detailed operation setup of the experiment is as follows:

- Because the experimental devices work in a negative pressure environment, system leak tests must be performed. In addition, the pressure-holding test must ensure that the pressure rise after the system is vacuumed does not exceed 15% within 24 h.
- Turn on the main power supply and the Programmable Logic Controller power, and ensure that the signal of each measuring instrument is correct.
- Turn on feed pump 11 and observe the position of the liquid surface in flash evaporator 8; then the second-effect circulation pump 9 is turned on after the position of the liquid surface reaches the lower observation lens. When the liquid surface reaches the upper observation lens, the discharge valve 13 is opened to feed the first effect. When the liquid position surface in flash evaporator 7 reaches the lower observation lens, the circulation pump 10 is turned on, and after reaching the upper observation lens, feed pump 11 and the second effect discharge valve 13 are turned off. After that, turn on the vacuum pump to allow the system to reach the required vacuum conditions.
- Turn on heat pump compressor 5, and steam is produced successively in the first effect and the second effect. When the concentration in the first effect reaches the requirement, the discharge valves 13 and 14 and the feed pump are turned on. We control the discharge flow through the

valve to maintain the liquid surface position in the flash evaporators and allow continuous system operation.

The concentration X_{in} of the ammonium sulfate solution feed in this experiment was 0.2, the discharge concentration was designed to be 0.47, and the feed temperature T_{in} was 25°C. The system is used for up to 8 h per test, and the experimental equipment is shown in Fig. 9, and the numbers in Fig. 9 corresponds to Fig. 1.

Fig. 10 compares the total pure water production and specific power consumption based on the results of multiple experiments. Among the 5 experiments, the difference between the highest pure water production and the minimum value is 4.87%, and the difference in specific power consumption is 6.8%. Since the second experimental result has an intermediate value, it is chosen for the next study.

Figs. 11 and 12 show the steam saturation temperature out of the first and second effects, respectively, and the compressor power of the heat pump varies with device runtime. From Fig. 11, we can determine that the first effect begins to evaporate at approximately 15 min, and the second effect begins to evaporate at approximately 30 min after the system starts because the first effect and the second effect require a period to increase the sensible heat of the solution before evaporation. After 40 min, the system can run stably. The steam saturation temperature of the first effect

is approximately 41°C, and the temperature of the second effect is approximately 31°C.

Fig. 12 shows that the power of the compressor is lower when the first effect evaporates only at the beginning. After the system is running stably, the power of the compressor fluctuates around 7.23 kW. Multiple experimental results indicate that the error range of the compressor power consumption is less than 5%; therefore, we believe that the results of this test are reliable. To calculate the evaporation rate of the system, we take the amount of discharged clean water after the end of running the system and divide it by the system's stable running time; the value obtained is the average evaporation rate of the system.

The results of the experimental test compared with those for the MVR system in the literature are shown in Table 2. Because the amount of refrigerant injected is higher than the design value, the evaporation rate of the experiment is 26% higher than the design value. However, the error of the specific power consumption is only 3.55%, which proves the reliability of the design method. According to the comparison between the indirect heat pump distillation and the MVR system, the specific power consumption of the compressor is slightly better than that of the single-effect MVR system, but it is higher than that of the double-effect MVR system. However, under the evaporation rate condition of this experiment, the MVR system must use a screw compressor

Fig. 9. Experimental device of the double-effect indirect heat pump distillation system.
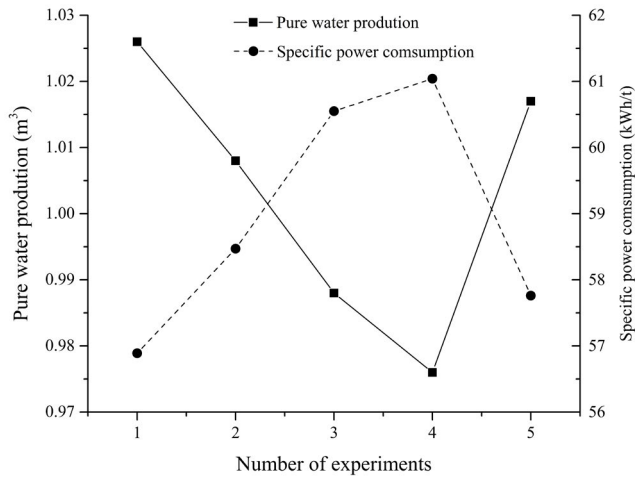
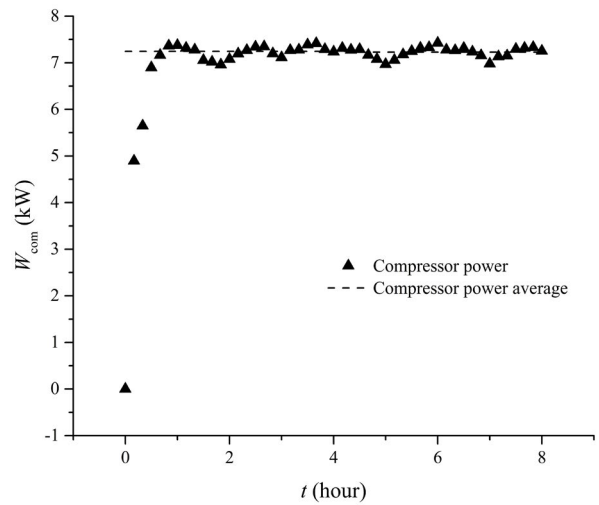Fig. 10. Comparison of the results of multiple experiments.

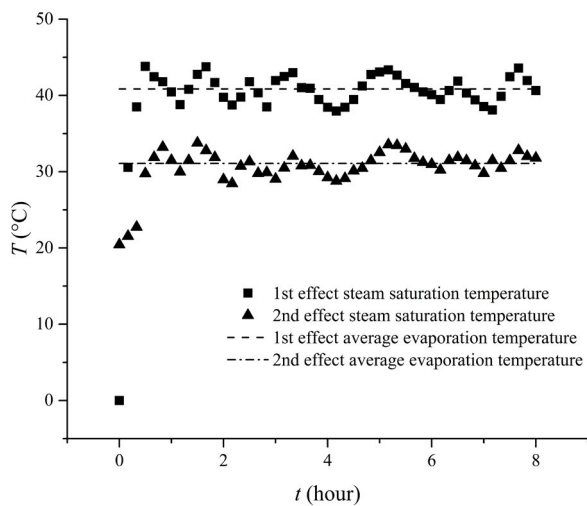Fig. 12. Change over time of the compressor power of the heat pump.

to satisfy the steam flow rate, and this type of compressor is several times higher than the price of the compressor in this experiment. The heat pump cycle is a closed-loop, which makes the system operation safer and easier.

Using the experimental results, we performed an exergy analysis on the system. The fluid positions of the system are marked in Fig. 13. The thermodynamic parameters of the fluid at each position are shown in Table 3.

As shown in Table 3, the reference state selected is the state of the feed ammonium sulfate solution with a temperature of 25°C, a pressure of 0.004 MPa and a concentration of 20% when we perform the exergy analysis calculation. The exergy destruction of the main equipment in the system is shown in Table 4. Among them, the compressor, evaporator, and condenser of the heat pump have the largest exergy destruction, which means most of the exergy loss of the system occurs in the heat pump cycle. The exergy efficiency of this system is 12.29%, meanwhile, the exergy efficiency of the two-stage MVR system [27] treated with the same concentration of ammonium sulfate solution was 12.04%. The

Fig. 11. Change in the steam saturation temperature over time for the first and second effects.

Table 2
Comparison of the system design and experimental parameters with an MVR system

| Parameters	Design	Experiment	Single-effect MVR system [24]	Double-effect MVR system [24]
Feed rate, kg h⁻¹	174	220	1,500	2,500
Evaporation rate, kg h⁻¹	100	126	1,200	2,000
Specific power consumption, kWh t⁻¹	55.73	58.47	58.6	41.5
Total heat transfer area, m²	20	20	96	166.5
Second effect saturated evaporation temperature, °C	30	31	–	70
Power of the compressor, kW	5.57	7.23	–	–
Power of the forced circulation pump of the first-effect, kW	0.16	0.64	–	–
Power of the forced circulation pump of the second-effect, kW	0.16	0.45	–	–
Compressor outlet pressure, MPa	1.755	1.8	–	–
Compressor inlet pressure, MPa	1.044	1.0	–	–
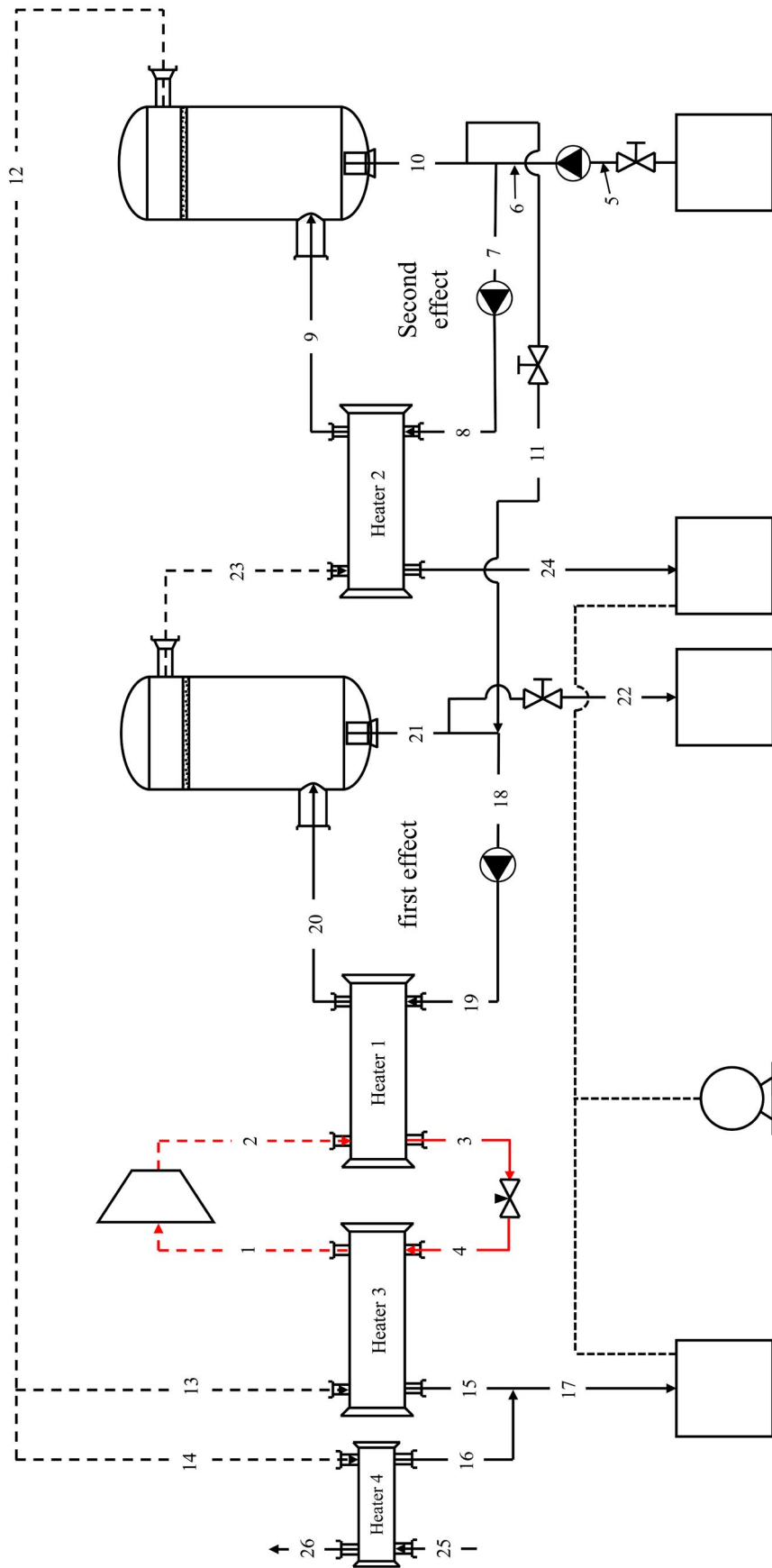
Fig. 13. System fluid location diagram.

Table 3
Thermodynamic parameters of fluids at each position

Position	Fluid	Mass flow rate/kg h^{-1}	Temperature/°C	Pressure/ MPa	Specific enthalpy/ kJ kg^{-1}	Mass concentration/%	Physical specific exergy/kJ kg^{-1}	Chemical specific exergy/kJ kg^{-1}	Total specific exergy/kJ kg^{-1}	Exergy/ kW
1	Gaseous R-22	802.438	27	1.0	414.764		−83.912	0	−83.912	−18.704
2	Gaseous R-22	802.438	74.35	1.8	444.339		−69.24	0	−69.24	−15.434
3	Liquid R-22	802.438	43.65	1.8	254.506		−82.6	0	−82.6	−18.411
4	Gas–liquid mixing R-22	802.438	25	1.0	254.506		−83.91	0	−83.91	−18.703
5	$(NH_4)_2SO_4$ solution	220	25	0.004		20	0	0	0	0
6	$(NH_4)_2SO_4$ solution	220	25	0.004		20	0.03	0	0.03	0.0018
7	$(NH_4)_2SO_4$ solution	10,220	30.8	0.004		27.66	0.195	1.595	1.79	5.0816
8	$(NH_4)_2SO_4$ solution	10,220	30.8	0.004		27.66	0.235	1.595	1.83	5.1952
9	$(NH_4)_2SO_4$ solution	10,220	34.34	0.004		27.66	0.655	1.595	2.25	6.3875
10	$(NH_4)_2SO_4$ solution	10,158.16	31.57	0.004		27.85	0.208	1.602	1.81	5.1073
11	$(NH_4)_2SO_4$ solution	158.16	31.57	0.004		27.85	0.208	1.602	1.81	0.0795
12	Steam	61.84	30	0.004	2,555.5		50.6362	0	50.6362	0.8698
13	Steam	54.93	30	0.004	2,555.5		50.6362	0	50.6362	0.7726
14	Steam	6.91	30	0.004	2,555.5		50.6362	0	50.6362	0.0972
15	Pure water	54.93	30	0.004	125.73		10.613	0	10.613	0.1619
16	Pure water	6.91	30	0.004	125.73		10.613	0	10.613	0.0204
17	Pure water	61.84	30	0.004	125.73		10.613	0	10.613	0.1823
18	$(NH_4)_2SO_4$ slurry solution	12,158.16	38.55	0.006		46.75	0.9	23.46	24.36	82.2702
19	$(NH_4)_2SO_4$ slurry solution	12,158.16	38.58	0.006		46.75	0.95	23.46	24.41	82.4391
20	$(NH_4)_2SO_4$ slurry solution	12,158.16	41.89	0.006		46.75	1.52	23.46	24.98	84.3641
21	$(NH_4)_2SO_4$ slurry solution	12,094	40.65	0.006		47	0.94	23.5	24.44	82.1048
22	$(NH_4)_2SO_4$ slurry solution	94	40.65	0.006		47	0.94	23.5	24.44	0.6382
23	Steam	64.16	36.57	0.006	2,567.4		101.564	0	101.564	1.8101
24	Pure water	64.16	36.57	0.006	153.2		11.363	0	11.363	0.2025
25	Water	2,008.34	25	0.101	104.83		10.443	0	10.443	5.8259
26	Water	2,008.34	27	0.101	113.19		10.467	0	10.467	5.8392

Table 4
Exergy destruction of the main equipment in the system

Equipment	Exergy destruction/kW	Proportion/%
Heater 1	1.053	14
Heater 2	0.415	6
Heater 3	0.611	8
Heater 4	0.063	1
Compressor	3.711	51
Flasher 1	0.449	6
Flasher 2	0.410	6
Other	0.570	8
Total	7.282	100

exergy efficiency of the two systems is closer but the exergy loss distribution is different, this is because the energy supply methods used in the two systems are essentially different. The forced circulation system in the MVR system is directly heated by the steam from the compressor; however, the forced circulation system studied in this paper is indirectly heated by the heat pump cycle. The advantage is that the closed heat pump cycle makes system operation easier, and the change in evaporation rate affecting the operation of the compressor during system operation is not a concern.

5. Conclusions

In the present paper, an indirect heat pump distillation system is proposed, which is established by a double-effect forced circulation distillation system combined with a refrigerant heat pump. A detailed calculation model of this system based on the mass and energy conservation equations is described, and the experimental setup is established to verify the results of the calculations and compare them to the energy-efficient MVR system. According to calculations, experiments, and exergy analysis, the following conclusions can be drawn:

- Feeding method has little effect on the performance index of the compressor, but the countercurrent feed method can achieve a lower compressor power and a lower total heat transfer area.
- Using R-22 as the working fluid of the heat pump enables a smaller heat transfer area and a higher performance index of the compressor. In addition, a lower compressor power and heat transfer area can be obtained when choosing a 25°C feeding temperature, which means a lower second effect saturated evaporation temperature will increase the initial investment of the system but reduce the energy consumption and maintenance costs.
- System runs stably by approximately 40 min after the heat pump compressor starts up. The error of the specific power consumption between the experimental and calculated values is 3.55%, which proves the reliability of the design method.
- Heat pump cycle is responsible for most of the exergy losses; among the heat pump components, the compressor accounts for more than half of total exergy losses.

- The specific energy consumption is slightly better than that of the single-effect MVR system but not as good as that of the double-stage MVR system. The exergy efficiency of the system studied in this paper is 12.29%, which is similar to that of the double-stage MVR system, but the exergy loss distributions of the two systems differ.

As a result, compared with direct heat pump methods such as MVR technology, the proposed system has advantages in terms of compressor manufacturing and maintenance costs and safety and convenience in operation, thus providing more choices for chemical production.

Symbols

A	—	Heat transfer area, m²
BPE	—	Boiling point elevation, °C
Cp	—	Specific heat at constant pressure, kJ kg⁻¹ K⁻¹
d	—	Tube diameter, m
e	—	Specific exergy, kJ kg⁻¹
E	—	Exergy, kW
F	—	Mass flow rate, kg s⁻¹
f	—	Correction factor, K² kg kJ⁻¹
h	—	Specific enthalpy, kJ kg⁻¹
k	—	Convective heat transfer coefficient, kW m⁻² °C⁻¹
M	—	Crystalline salt, kg
P	—	Pressure, kPa
Q	—	Rate of heat transfer, kW
R	—	Fouling resistance
R_g	—	Gas constant of R-22, kJ kg⁻¹ K⁻¹
T	—	Temperature, K
U	—	Overall coefficient of heat transfer, kW m⁻² °C⁻¹
v	—	Specific volume, m⁻³ kg⁻¹
W	—	Power, kW
X	—	Mass concentration, %
x	—	Molar fraction, %
α	—	Performance index of the compressor, K kJ⁻¹ kg⁻¹
γ	—	Latent heat; kJ kg⁻¹
η	—	Compressor efficiency
ε	—	Pressure ratio
λ	—	Thermal conductivity, kW m⁻¹ °C⁻¹

Subscripts

ad	—	Adiabatic
b	—	Brine
c	—	Condensation
ch	—	Chemical
com	—	Compressor
cr	—	Critical
d	—	Destruction
E	—	Exergy
e	—	Evaporation
ej	—	Flash evaporator of the *j*th effect
h	—	Heater
i	—	Inside of the tubes
in	—	Inlet
o	—	Outside of the tubes
out	—	Outlet
p	—	Pump
ph	—	Physical

r — Refrigerant
rc — Refrigerant under condensing pressure
s — Solid
v — Vapor
v1 — Vapor of the first effect
v2 — Vapor of the second effect
w — Water

Acknowledgments

References

[1] F. Kargi, Enhanced biological treatment of saline wastewater by using halophilic bacteria, Biotechnol. Lett., 24 (2002) 1569–1572.
[2] O. Lefebvre, R. Moletta, Treatment of organic pollution in industrial saline wastewater: a literature review, Water Res., 40 (2006) 3671–3682.
[3] D. Aussenac, S. Domenech, M. Enjalbert, Mathematical model of a mechanical vapor compression evaporator. Application to seawater desalting. Part I - The model settlement, Desalination, 41 (1982) 137–169.
[4] D. Han, C. Yue, W. He, L. Liang, W. Pu, Energy-saving analysis for a solution evaporation system with high boiling point elevation based on self-heat recuperation theory, Desalination, 355 (2015) 197–203.
[5] M. Ahmadi, E. Baniasadi, H. Ahmadikia, Process modeling and performance analysis of a productive water recovery system, Appl. Therm. Eng., 112 (2017) 100–110.
[6] D. Han, W.F. He, C. Yue, W.H. Pu, Study on desalination of zero-emission system based on mechanical vapor compression, Appl. Energy, 185 (2017) 1490–1496.
[7] A.M. Helal, S.A. Al-Malek, Design of a solar-assisted mechanical vapor compression (MVC) desalination unit for remote areas in the UAE, Desalination, 197 (2006) 273–300.
[8] D. Zejli, A. Ouammi, R. Sacile, H. Dagdougui, A. Elmidaoui, An optimization model for a mechanical vapor compression desalination plant driven by a wind/PV hybrid system, Appl. Energy, 88 (2011) 4042–4054.
[9] K. Alexander, B. Donohue, T. Feese, G. Vanderlinden, M. Kral, Failure analysis of an MVR (mechanical vapor recompressor) impeller, Eng. Fail. Anal., 17 (2010) 1345–1358.
[10] B.F. Lachner, G.F. Nellis, D.T. Reindl, The commercial feasibility of the use of water vapor as a refrigerant, Int. J. Refrig., 30 (2007) 699–708.
[11] W. Rice, D.S.C. Chau, Freeze desalination using hydraulic refrigerant compressors, Desalination, 109 (1997) 157–164.
[12] V.V. Slesarenko, Desalination plant with absorption heat pump for power station, Desalination, 126 (1999) 281–285.
[13] V.V. Slesarenko, Heat pumps as a source of heat energy for desalination of seawater, Desalination, 139 (2001) 405–410.
[14] J. Chen, S. Huang, A discussion of "heat pumps as a source of heat energy for desalination of seawater", Desalination, 169 (2004) 161–165.
[15] A.A.A. Attia, New proposed system for freeze water desalination using auto reversed R-22 vapor compression heat pump, Desalination, 254 (2010) 179–184.
[16] A.A.A. Attia, Heat pump seawater distillation system using passive vacuum generation system, Desalination, 397 (2016) 151–156.
[17] M.H. Sharqawy, J.H. Lienhard, S.M. Zubair, On exergy calculations of seawater with applications in desalination systems, Int. J. Therm. Sci., 50 (2011) 187–196.
[18] K.S. Spiegler, Y.M. El-Sayed, The energetics of desalination processes, Desalination, 134 (2001) 109–128.
[19] G. Zuo, R. Wang, R. Field, A.G. Fane, Energy efficiency evaluation and economic analyses of direct contact membrane distillation system using Aspen Plus, Desalination, 283 (2011) 237–244.
[20] N. Kahraman, Y.A. Cengel, Exergy analysis of a MSF distillation plant, Energy Convers. Manage., 46 (2005) 2625–2636.
[21] A. Piacentino, F. Cardona, Advanced energetics of a multiple effects evaporation (MEE) desalination plant: Part I: 2nd principle analysis by a zooming representation at single-effect level, Desalination, 264 (2010) 84–91.
[22] A. Piacentino, E. Cardona, Advanced energetics of a multiple-effects-evaporation (MEE) desalination plant. Part II: potential of the cost formation process and prospects for energy saving by process integration, Desalination, 259 (2010) 44–52.
[23] C.-Z. Jin, Q.-L. Chou, D.-S. Jiao, P.-C. Shu, Vapor compression flash seawater desalination system and its exergy analysis, Desalination, 353 (2014) 75–83.
[24] L. Liang, D. Han, R. Ma, T. Peng, Treatment of high-concentration wastewater using double-effect mechanical vapor recompression, Desalination, 314 (2013) 139–146.
[25] K. Srinivasan, Choice of vapor-compression heat pump working fluids, Int. J. Energy Res., 15 (1991) 41–47.
[26] L. Fitzsimons, B. Corcoran, P. Young, G. Foley, Exergy analysis of water purification and desalination: a study of exergy model approaches, Desalination, 359 (2015) 212–224.
[27] N. Sato, Chemical Energy, and Exergy: An Introduction to Chemical Thermodynamics for Engineers, Elsevier, Amsterdam, 2004.
[28] L.Z. Wei, Design and Experimental Research on Heat Pump Seawater Desalination Plant, Chongqing University, 2016. (In Chinese)

Appendix: calculation of the physical and chemical exergy

Stream 8 in Fig. 13 is used as a numeric example. The state parameters of the ammonium sulfate solution at this point are 30.8°C and 0.004 MPa with a mass concentration of 27.66%. The reference state assumed for calculations is 25°C and 0.004 MPa with a mass concentration of 20%. According to Eq. (27), the specific physical exergy of stream 8 is calculated by:

$$e_{ph} = Cp\left[T - T_0 - T_0 \ln\left(\frac{T}{T_0}\right)\right] + v(P - P_0) \tag{A1}$$

where $v(P - P_0)$ means the work of the circulation pump to increase the exergy value of the fluid, which can be calculated by:

$$\frac{W_{pump2} \cdot \eta_{pump2}}{q} = \frac{0.45 \times 0.25 \times 3,600}{10,220} = 0.04 \text{ kJ / kg} \tag{A2}$$

$$Cp\left[T - T_0 + \ln\left(\frac{T}{T_0}\right)\right] = \left[Cp_w \cdot (1 - X) + Cp_s \cdot X\right] \cdot$$

$$\left[T - T_0 + \ln\left(\frac{T}{T_0}\right)\right] = \left[4.18 \times (1 - 0.2766) + 1.7 \times 0.2766\right] \times \tag{A3}$$

$$\left\{30.8 - 25 + \left[\ln\frac{(30.8 + 273.15)}{(25 + 273.15)}\right]\right\} = 0.195 \text{ kJ / kg}$$

$$e_{ph} = 0.04 + 0.195 = 0.235 \text{ kJ kg}^{-1}$$

The specific chemical exergy of stream 8 is calculated by:

$$e_{ch} = \overline{R}T_0 \sum_1^k x_{i0} \ln\left(\frac{\alpha_{i0}}{\alpha_i^0}\right) \tag{A4}$$

The ammonium sulfate solution is treated as a one-component electrolyte solution, and the activity α of electrolyte MX is expressed as $\alpha = \gamma_{MX} \cdot x$, where x is the molar concentration of electrolyte MX and the average activity coefficient γ_{MX} is calculated by [26]:

$$\ln \gamma_{MX} = \left| Z_M \cdot Z_X \right| \cdot f^{\gamma} + \left(\frac{2 v_M \cdot v_X}{v} \right) \cdot m_k \cdot$$

$$B_{MX}^{\gamma} + \left(\frac{2 \left(v_M \cdot v_X \right)^{3/2}}{v} \right) \cdot m_k^2 \cdot C_{MX}^{\gamma} \tag{A5}$$

where M and X represent cations and anions, respectively; n_M and n_X are the numbers of cations and anions in a single molecule; Z_M and Z_X are the numbers of electric charges carried by cations and anions in a single molecule; m_k is the ratio of the amount of solute to the mass of solvent; and the coefficients f^{γ}, B_{MX}^{γ}, and C_{MX}^{γ} are calculated by:

$$f^{\gamma} = -A^{\phi} \left[\frac{I^{1/2}}{\left(1 + b \cdot I^{1/2} \right)} + \frac{2}{b} \cdot \ln \left(1 + b \cdot I^{1/2} \right) \right] \tag{A6}$$

$$B_{MX}^{\gamma} = 2\beta_{MX}^{(0)} + \beta_{MX}^{(1)} \cdot g \left(\alpha_1 \cdot I^{1/2} \right) + \beta_{MX}^{(2)} \cdot g \left(\alpha_2 \cdot I^{1/2} \right) \tag{A7}$$

$$C_{MX}^{\gamma} = 1.5 C_{MX}^{\phi} \tag{A8}$$

where b and α_1 are 1.2 and 2 for ammonium sulfate solution, and A^{ϕ} is the Debye–Hückel coefficient, which can be calculated by:

$$A^{\phi} = \frac{1}{3} \left(\frac{2\pi N_0 \rho_w}{1,000} \right)^{1/2} \left(\frac{e^2}{DkT} \right)^{3/2} \tag{A9}$$

where N_0 is Avogadro's constant; ρ_w is the density of the solvent at temperature T; e is the electron charge; D is the permittivity of the solvent; and k is the Boltzmann constant.

Table A1
Pitzer parameters of ammonium sulfate

Substance	$\beta_{MX}^{(0)}$	$\beta_{MX}^{(1)}$	$\beta_{MX}^{(2)}$	C_{MX}^{ϕ}
Ammonium sulfate	0.04841	1.1324	0	−0.00155

In addition, $\beta_{MX}^{(0)}$, $\beta_{MX}^{(1)}$, $\beta_{MX}^{(2)}$, and C_{MX}^{ϕ} are Pitzer parameters, and the Pitzer parameters of ammonium sulfate are shown in Table A1.

The expression of $g(x)$ is:

$$g(x) = 2 \left[1 - \left(1 + x - \frac{1}{2} x^2 \right) e^{-x} \right] \Big/ x^2 \tag{A10}$$

The formula for calculating the ionic strength I is

$$I = \frac{1}{2} \sum m_{ki} Z_i^2 \tag{A11}$$

According to the above equations, the average activity coefficient of ammonium sulfate at the reference concentration is calculated as $\gamma_0 = 0.172$, and at a concentration of 27.66%, $\gamma = 0.232$. The average activity coefficient of water is 1. The molar concentrations of the reference state and calculation state solutes are 0.033 and 0.0495. The specific chemical exergy of stream 8 is:

$$\begin{aligned}
e_{ch} &= \left[\frac{\left(8.314 \times 298.15 \right)}{18.016} \right] \times 0.9505 \times \ln \left[\frac{\left(1 \times 0.967 \right)}{\left(1 \times 0.9505 \right)} \right] \\
&+ \left[\frac{\left(8.314 \times 298.15 \right)}{132.14} \right] 0.0495 \times \ln \left[\frac{\left(0.172 \times 0.033 \right)}{\left(0.232 \times 0.0495 \right)} \right] \\
&= 1.595
\end{aligned} \tag{A12}$$

Consequently, the specific exergy $e = e_{ph} + e_{ch} = 0.235 + 1.595 = 1.83$ kJ kg^{-1}.